Medical Engineering and Physics 69 (2019) 140–146

Contents lists available at ScienceDirect

Medical Engineering and Physics

journal homepage: www.elsevier.com/locate/medengphy

Communication

Moderate thickness of lipid core in shoulder region of atherosclerotic plaque determines vulnerable plaque – A parametric study

Stanislav Polzer[a,*], Anna Polišenská[b], Kamil Novák[c], Jiří Burša[b]

[a] Department of Applied Mechanics, VŠB-Technical University of Ostrava, 17. Listopadu 15, Ostrava Poruba 708 33, Czech Republic
[b] Institute of Solid Mechanics, Mechatronics and Biomechanics, Brno University of Technology, Technicka 2896/2Brno, 616 00, Czech Republic
[c] TRW Automotive Czech s.r.o., Na Roli 2405/26, Jablonec nad Nisou 466 01, Czech Republic

ARTICLE INFO

Article history:
Received 11 June 2018
Revised 10 April 2019
Accepted 14 April 2019

Keywords:
Atherosclerotic plaque
Finite element analysis
Parametric study

ABSTRACT

Peak stress in the fibrous cap of atherosclerotic plaque is largely determined by the cap thickness which cannot be accurately estimated in vivo. This parametric study investigates idealized atherosclerotic plaque geometries. Finite element modeling is applied to search for larger morphological features associated with high cap stresses. By varying seven geometrical and two loading parameters, 100 3D model geometries of atherosclerotic plaques in common iliac artery were generated. In each model peak cap stress was calculated, and statistical comparison of the geometries generating the highest and lowest peak cap stresses was performed. The analysis showed that, compared to geometries generating the lowest stresses, those with high peak cap stress had a significantly lower cap thickness, higher stenosis ratio, lower relative lipid core volume, and cap shoulder radius larger than lipid core radius. High cap stress was observed for cap thicknesses up to 0.13 mm. It can be concluded that vulnerable plaques contain thin fibrous cap, large stenosis ratio and only moderate small-radius lipid core which reaches the shoulder region of the fibrous cap.

1. Introduction

Atherosclerosis is a progressive vascular disease which manifests itself as a progressive thickening of intimal layer due to lipid accumulation under endothelium cells. Rupture of the atherosclerotic plaque is associated with blood clot formation which then occludes this artery or some thinner artery downstream. According to the type of the affected artery, this may cause myocardial infarction [1] (coronary arteries), or stroke [2] (carotid arteries) which are leading causes of death in developed countries [3]; in iliac or femoral arteries it results in acute lower limb ischemia [4]. Therefore researchers have devoted a great effort to identification of vulnerable plaques in the last two decades. Besides clinical, biochemical, and histological observations [2], biomedical engineering plays also an important role in this effort. Specifically, there are hundreds of studies where stress in the atherosclerotic cap is investigated (see the review by Holzapfel et al. [5] and references therein) mostly via finite element analysis (FEA) or fluid structure interaction (FSI) analysis [6,7]. FSI is more complex compared to FEA and can provide more realistic spatial pressure distribution and wall shear stress distributions [6,7] in exchange for much longer computational times. Consequently, only a very limited number of geometries can mostly be investigated in one study [6,8,9]. In contrast, 2D FEAs [5,10] are by several orders faster but they intrinsically simplify the state of stress and neglect the axial morphology of the atherosclerotic plaque which may be determining for identification of its weakest spot [11,12]. Finally, the 3D FEA studies were performed on both patient-specific [9,13] and idealized [14,15] geometries. Although the patient-specific geometry is crucial in estimating vulnerability of an individual plaque, it is usually performed with a low number of patients and the morphological features associated with vulnerability can hardly be specified due to the irregular geometry. This makes generalization of results difficult.

Computational studies show consistently that peak stress in the fibrous cap covering the lipid core of the atherosclerotic plaque can serve as an indicator of the vulnerable plaques [14,16–18]. The stress is affected by several morphological factors, with fibrous cap thickness f_c being the most important among them. Although there is evidence for an inverse exponential relation between f_c and peak cap stress [19,20], the importance of this observation for clinical practice is limited because f_c values associated with dangerous stresses (threshold of 300 kPa is based on the work of Cheng et al. [17]) are mostly far below the current resolution of magnetic resonance imaging (MRI) [21]. Consequently, clinicians cannot safely

* Corresponding author.
E-mail addresses: polzer@seznam.cz (S. Polzer), kamil.novak1@trw.com (K. Novák), bursa@fme.vutbr.cz (J. Burša).

https://doi.org/10.1016/j.medengphy.2019.04.011
1350-4533/

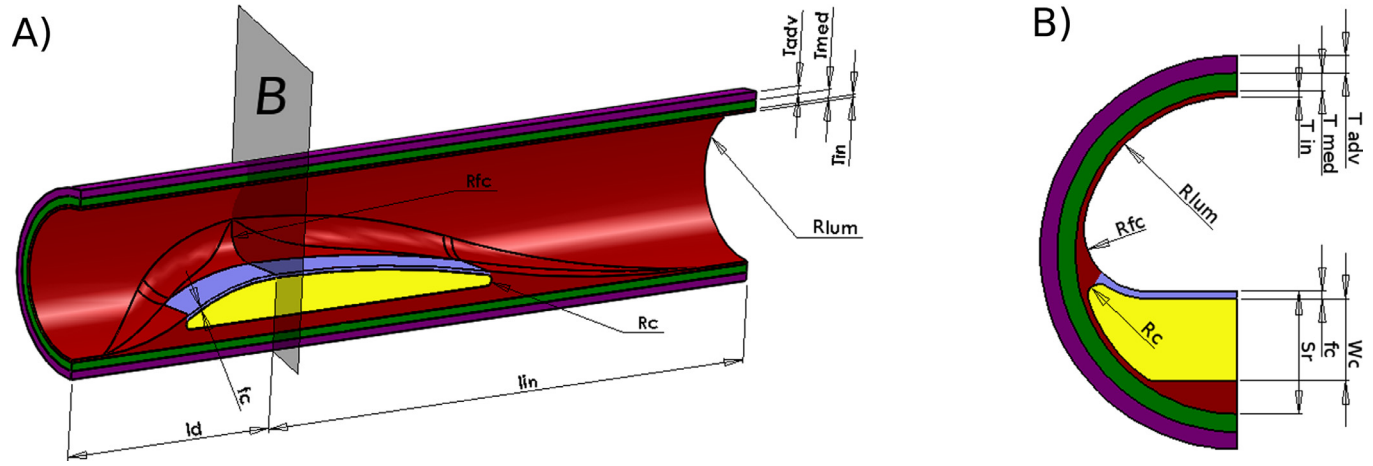

Fig. 1. Idealized geometry of common iliac artery. Only a half is used due to symmetry. Intima with atheroma plaque marked red, fibrous cap blue, lipid core yellow, media green and adventitia purple. (A) A complete 3D model. (B) Cross section at the maximal stenosis.

determine whether the investigated plaque contains a dangerously thin cap or not. A possible way how to overcome this limitation is to search for other morphological parameters (larger in dimensions) which could be associated with high cap stresses and also quantified via current imaging techniques with a lower relative uncertainty.

In this preliminary study we investigate the effect of 3D morphology of atherosclerotic plaques on the peak cap stress with the aim to identify morphological features which are decisive for its magnitude.

2. Methods

2.1. Idealized geometry

In order to identify the parameters decisive for the plaque vulnerability, i.e., those inducing high peak cap stress, we used FEA performed on idealized 3D geometries. This approach allows us to analyze a large number of cases with clearly defined morphology. Our hypothesis could be tested with any artery prone to atherosclerosis but, as emphasized recently [5], the importance of using relevant constitutive models in FEAs reduces substantially the possible choice; the models should be fitted to experimental data obtained with the same type of artery as the modeled one. Therefore we decided to analyze atherosclerotic plaques in common iliac artery (CIA) for which mechanical responses of individual components of atherosclerotic plaque (based on standard uniaxial tensile testing) were published [22].

An idealized parametric 3D model of CIA was created in software Solidworks 2012 (Dassault Systems, Vélizy-Villacoublay, France) as shown in Fig. 1. The chosen geometry aimed at mimicking a real iliac atherosclerotic artery (see Fig. 1 in Holzapfel et al. [23]) and was assumed to be symmetric along an axial plane; thus only one half was modeled (see Fig. 1A). Radius of the lumen was chosen to be $R_{lum} = 4$ mm. The total wall thickness was set to 1.05 mm and the portions of intima, media and adventitia thicknesses in the healthy part of CIA were kept to 14%, 44%, and 42%, respectively, according to experimental measurements [24]. To enable a direct comparison with patient-specific cases in the future, this geometry was considered as loaded and a reconstruction of the unloaded geometry was realized as described below.

The atheroma plaque was modeled with the mutually independent lengths of its upstream l_{in} and downstream l_d parts (see Fig. 1A). Their ranges from 4 to 40 mm cover all possible plaque lengths in CIA. Transition between the intima and atheroma in transversal planes was realized using radius R_{fc}. The lipid core was modeled with maximal thickness W_c being independent of the thickness of the atheroma and its edges were rounded with radius R_c. It is noted the parameter W_c determines also the lipid core length in axial direction since it is modeled to fill the whole space between fibrous cap and the line distant by W_c from the point of maximal stenosis. This choice was made to keep the number of parameters reasonable. Additionally, the lipid core geometry can be described by two derived (dependent on W_c) ratios K_{ax} and K_{circ}, defined as percentages of the plaque filled with lipid in the longitudinal plane (symmetry plane in Fig. 1B) and in the cross section plane (plane of the cross section in Fig. 1A), respectively. These parameters were used for better comparison of the obtained results with other studies. Considered ranges of the individual variables are specified in Table 1.

Table 1
Values of parameters used to generate the geometries and loads of the FE models.

Parameter	Symbol	Units	Value (for constants) or range (for variables)
Thickness of the healthy intima	T_{in}	[mm]	0.15
Thickness of the healthy media	T_{med}	[mm]	0.46
Thickness of the healthy adventitia	T_{adv}	[mm]	0.44
Length of the increasing part	l_{in}	[mm]	⟨4, 40⟩
Length of the decreasing part	l_d	[mm]	⟨4, 40⟩
Radius of the lumen without stenosis	R_{lum}	[mm]	4
Radius of the fibrous cap shoulder	R_{fc}	[mm]	⟨0.1, 3.5⟩
Thickness of the fibrous cap	f_c	[mm]	⟨0.02, 0.4⟩
Thickness of the lipid core	W_c	[mm]	⟨0.2, 5⟩
Percentage of the lipid core area in the cross section (dependent)	K_{circ}	[%]	⟨7, 87⟩
Percentage of the lipid core area axially (dependent)	K_{ax}	[%]	⟨0.6, 87⟩
Stenosis	S_r	[%]	⟨6, 75⟩
Radius of the lipid core	R_c	[mm]	⟨0.1, 1.5⟩
Axial pre-strain	ε_a	[%]	⟨0, 10⟩
Blood pressure	*pres*	[kPa]	⟨10, 15⟩

2.2. Material models

We used hyperelastic incompressible constitutive models to describe mechanical behavior of the individual layers or components. The experimental uniaxial stress-stretch curves for each individual component reported by Holzapfel et al. [22] were averaged across

Table 2
Applied constants of the constitutive models for all the considered components of the wall and atherosclerotic plaque. All the parameters are based on the experimental data from Holzapfel et al. [22].

Layer	Constants					
	c_{10} [kPa]	c_{20} [kPa]	c_{30} [kPa]	k_1 [kPa]	k_2 [-]	ϕ [rad]
Intima	10	740	0	0	–	–
Fibrous cap	100	537	0	0	–	–
Media (anisotropic)	8.5	27	0	21	2	0.027
Adventitia	10	0	10,422	0	–	–
Lipid core	0.01	0	0	0	–	–

the stresses for all the tested patients to construct their mean axial and circumferential responses. Then the chosen constitutive model was fitted to these mean response curves. For the media we used anisotropic constitutive model characterized by combination of isotropic Yeoh type strain energy density function (SEDF) and anisotropic Holzapfel Gasser Ogden (HGO) model [25]:

$$\psi_{iso} + \psi_{aniso} = \sum_{i=1}^{3} c_{i0}(I_1 - 3)^i + \sum_{j=4,6} \frac{k_1}{2k_2}\left(e^{k_2(I_j-1)^2} - 1\right) \quad (1)$$

Here c_{i0} are stress-like material constants describing the isotropic response of the tissue, k_1 is a stress-like constant defining the stiffness of collagen fibers, and k_2 refers to their stiffening during deformation. I_1 is the first invariant of the right Cauchy-Green deformation tensor C, $I_4 = \boldsymbol{a_0} \cdot \boldsymbol{Ca_0}$ and $I_6 = \boldsymbol{b_0} \cdot \boldsymbol{Cb_0}$ are the invariants related to two families of fibers; here $\boldsymbol{a_0} = (\sin\phi,\ \cos\phi,\ 0)$ and $\boldsymbol{b_0} = (\sin\phi,\ -\cos\phi,\ 0)$, with ϕ representing the angle between each fiber family and the circumferential direction. For the other components of the wall and plaque, the anisotropic part of the described SEDF was set to zero since either their anisotropy is much less pronounced compared to inter-patient variability (intima, adventitia, fibrous cap [26]), or isotropy is generally accepted (lipid core). All constants for all the components are specified in Table 2.

2.3. Finite element model setup

Although the model geometry is highly simplified, the problem cannot be solved analytically on the basis of Euler-Lagrange equations; their discretized solution, together with strain-displacement and constitutive equations, is found using finite element method (FEM) [30]. The created geometry of each model was uploaded into ANSYS 17.2. (Ansys Inc. USA) and meshed with quadratic hexahedral elements (media and adventitia), quadratic tetrahedral elements (intima with atherosclerotic plaque) or linear tetrahedral elements (lipid core). The maximal element size was prescribed for all volumes, with element refinement close to radiuses on the basis of the performed mesh convergence analysis (see Fig. 2). A typical finite element (FE) mesh is shown in Fig. 2A, consisting of 110k nodes. The media and adventitia were connected by sharing nodes on the interface while the intima was connected with both media and the lipid core through a bonded contact. The fibrous cap was created by changing the material parameters of the elements of intima layer covering the lipid core (see Table 2), thus no contact was necessary.

Blood pressure *pres* and axial pre-strain ε_a were used as variables in this study (see Table 1). The pressure was applied as a constant value on the luminal surface of the geometry. Comparison with the computationally much more demanding FSI analyses [8,27] demonstrated that this simplification does not affect the results significantly, except for the wall shear stress. However, this stress is very low and consequently negligible from the point of view of the rupture risk; it might become relevant only if its impact on remodelation of endothelial cells was investigated.

In contrast to the pressure, ε_a was prescribed in a more complex way. Both ends of the artery were constrained only in the circumferential direction, and the axial displacement of each (*i*th) node U_{ai} of the media and adventitia was prescribed as function of its position:

$$U_{ai} = (loc_{ai} - loc_{a\,\min})\varepsilon_a/100 \quad (2)$$

where loc_{ai} refers to the axial coordinate of the (*i*th) node, $loc_{a\min}$ is the minimal axial coordinate in the whole geometry and ε_a is the prescribed percentage of axial pre-strain. Eq. (2) makes the axial pre-strain constant along the length of the artery, independently of differences in its local stiffness. Finally, the displacements of the symmetry plane were suppressed in its normal direction.

A non-linear static structural solution was performed using direct sparse solver with default setting of convergence criteria. Newton–Raphson iterative scheme was used for non-linear solution, and an automatic gradual increase of the applied loads was prescribed via sub-steps. At the first sub-step the load was 0.02 of the final values of both *pres* and ε_a, and this value increased by 50% in every following sub-step until the final load values were reached. This setup respects the nonlinear gradually stiffening nature of the arterial wall materials, and prevents an excessive mesh deformation during the initial sub-steps. More information on the solution procedure can be found elsewhere [28].

Since we expect future comparison of our results with patient-specific geometries, an analogical procedure was applied to recalculate the created geometry into its shrank (unloaded) shape. The reason is that the real patient-specific geometries (reconstructed on the basis of computed tomography angiography (CT-A) or MRI) are not load free but deformed due to presence of the intraluminal pressure *pres* and axial pre-strain ε_a. Reconstruction of the shrank geometry was solved by a repeated application of standard (forward) FE method (as implemented in ANSYS) when the calculated displacements induced by the increase of *pres* and ε_a were subtracted from the investigated geometry to obtain its unloaded shape. In each step the equilibrium was checked and differences between the loaded and original recorded geometries were compared until they became negligible (typically after some 10 iterations). Details on this modification of the so called backward incremental method can be found elsewhere [29].

2.4. Parametric study

For the parametric study we have generated 100 FE models in which we varied *pres*, ε_a, and 7 independent geometric parameters (l_{in}, l_d, R_{fc}, f_c, W_c, S_r, R_c). Their ranges are specified in Table 1. The chosen combinations of the parameters were generated using Latin hypercube sampling method [31] to cover the input space uniformly. Solution of one case took from 4 to 12 h using a 6 core 3.2 GHz PC with 32 GB RAM.

For each of the solved FE models the maximal 1st principal nodal Cauchy stress in the fibrous cap σ_{cap} was stored and our FE models were ranked according to this σ_{cap}. On the basis of mean Cauchy ultimate stresses estimated from tensile tests in circumferential direction of the fibrous cap [26], the threshold of $\sigma_{cap} > 255\ kPa$ was chosen to define a subgroup of geometries considered as risky. Their morphological features were extracted (see Table 3) and compared with those in the subgroup of the same size characterized by the lowest σ_{cap}. Here we used non-parametric Man-Whitney test [32] with the null hypothesis assuming there is no difference in parameters between both subgroups and the alternative hypothesis stating parameters are higher in one of them.

3. Results

The results showed the maximal σ_{cap} values occurred in the transversal section of the maximal stenosis in the geometries with

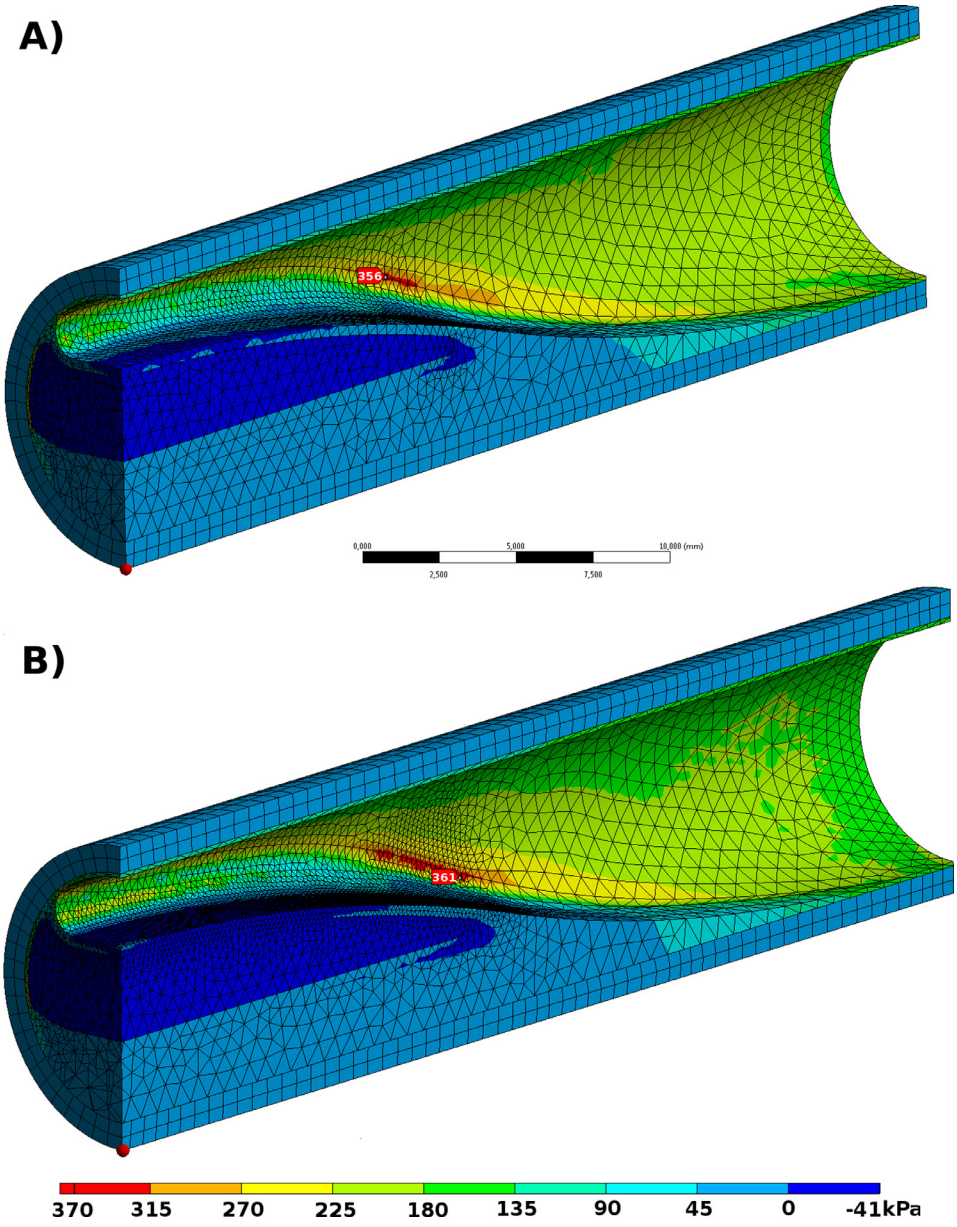

Fig. 2. Sensitivity check of FE mesh. 1st principal stress distribution in the upstream half of the model obtained with the mesh size used in all analyses (A) with one quadratic element across the cap thickness and the element size in the fibrous cap shoulder set to a half of its radius which resulted in 110k of nodes and 77k of elements. Peak stress is 356 kPa and σ_{cap} (on the inner side, not visible in the figure) is 103 kPa. The same model with a finer mesh (B) with two elements across the cap and element size in the fibrous cap shoulder set to a quarter of its radius resulted in 164k nodes and 132k elements. With this mesh the peak stress raised to 361 kPa only (by 1,4%) and σ_{cap} changed also negligibly.

Table 3
Results of statistical analysis of the selected subgroups of geometries showing the highest and lowest σ_{cap} with their morphological parameters and the calculated *p*-values. Median, 1st (Q1) and 3rd (Q3) quartile values are reported for all parameters and these values are compared statistically with the significant results marked in bold.

Subgroup definition (no. of geometries)		Morphological features										
		ε_a [−]	*pres* [kPa]	R_{fc} [mm]	S_r [%]	f_c [mm]	l_d [mm]	l_{in} [mm]	R_c [mm]	W_c [mm]	K_{ax} [%]	K_{circ} [%]
$\sigma_{cap} > 255kPa$	Med.	4.3	12.6	1.0	62.9	0.07	17.8	22.8	0.3	1.4	11.5	25.1
$n = 10$	Q1	2.7	11.5	0.8	59.6	0.04	15.3	19.0	0.2	1.2	4.5	17.4
	Q3	7.9	14.5	1.4	70.9	0.11	32.0	32.9	0.6	2.7	38.1	58.3
σ_{cap}low	Med.	3.7	13.4	0.5	49.1	0.25	24.1	18.1	0.8	2.6	39.3	62.3
$n = 10$	Q1	2.2	10.6	0.4	45.4	0.16	10.3	14.3	0.5	2.0	27.8	48.6
	Q3	5.8	13.6	0.7	51.7	0.29	29.5	24.4	0.9	3.0	62.4	73.3
p-value		0.25	0.21	**0.017**	**0.013**	**0.0003**	0.312	0.093	**0.009**	**0.004**	**0.019**	**0.013**

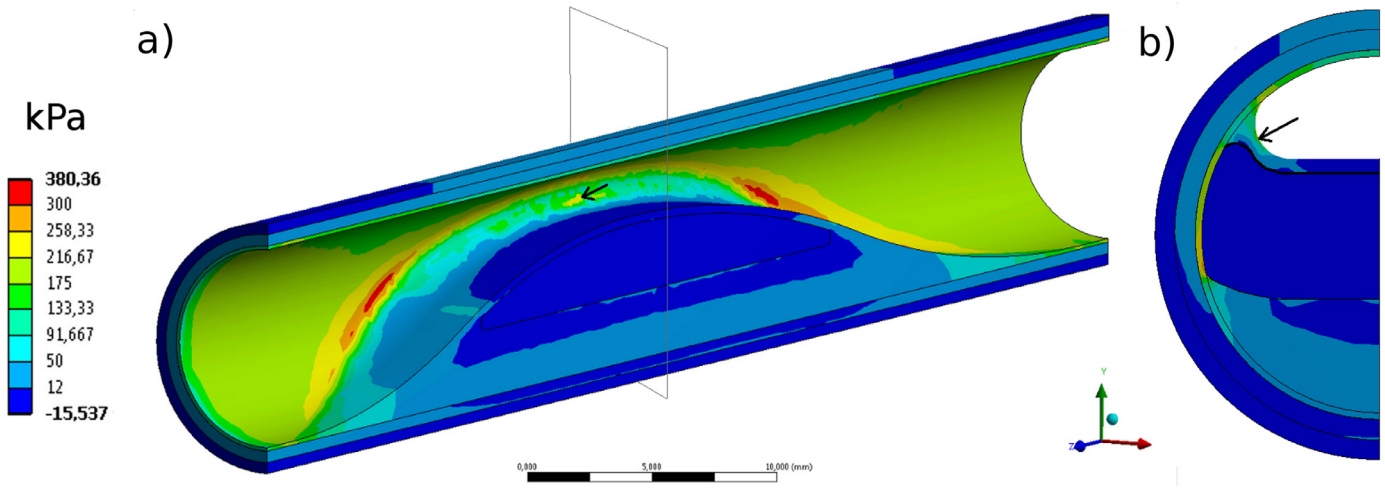

Fig. 3. 1st principal Cauchy stress distribution in a typical geometry where σ_{cap} (arrow) is located at the maximal stenosis. It occurs when lipid core takes part of the shoulder region B). The geometry is defined by: $W_c = 2.8$ mm, $S_r = 71\%$, $l_{in} = 38$ *mm*, $l_d = 29$ *mm*, $R_c = 0.32$ *mm*, $K_{ax} = 30.8\%$, $K_{circ} = 52.3\%$, $R_{fc} = 0.8$ *mm*, $f_c = 0.34$ *mm*, $pres = 11$ *kPa* and $\varepsilon_a = 7\%$. A) Global view showing the peak wall stress located out of the area of maximal stenosis and thus not aligned with the σ_{cap} (arrow). B) Transversal cut at the area of maximal stenosis.

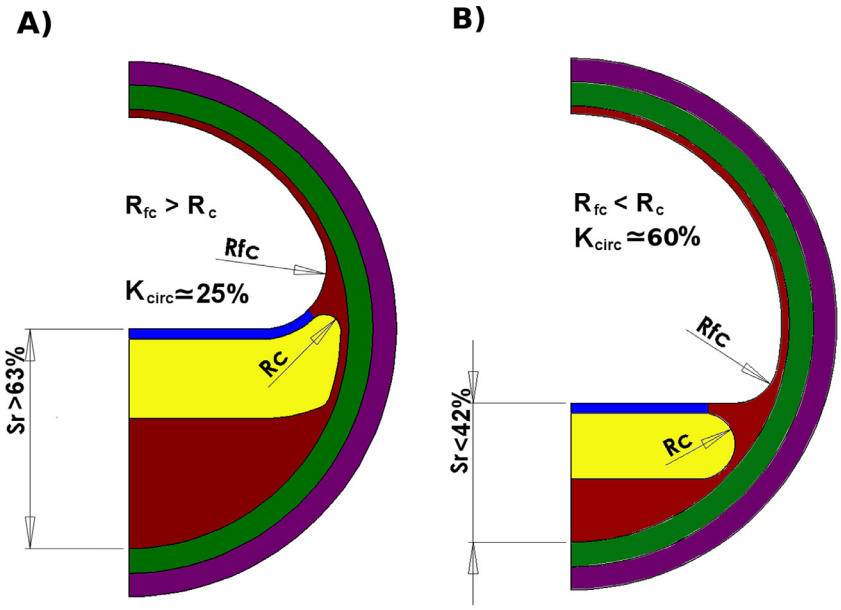

Fig. 4. Typical examples of combinations of geometrical parameters (excluding cap thickness f_c) which generate either risky (A) or safe (B) atherosclerotic plaque geometries. (A) Geometry is risky due to high stenosis ratio S_r, moderate lipid core thickness ratios K_{ax} and K_{circ}, and lipid core interfering with the shoulder region which is characterized by $R_{fc} > R_c$. (B) Non risky geometry is characterized by $R_{fc} < R_c$, low S_r and also relatively larger lipid core described by K_{ax} and K_{circ}.

$R_c < R_{fc}$ in which the lipid core reached the shoulder region, see Fig. 3B. In the other cases this location did not coincide with the point of maximal stenosis and it occurred near one of the axial ends of the lipid core. This observation was consistent in all the analyzed cases.

3.1. Statistical analysis

Analysis of correlation between subgroups of geometries which generated either the highest (median 307 kPa) or lowest (median 22 kPa; $p = 10^{-4}$) σ_{cap} revealed (see Table 3) that a typical risky geometry had a significantly larger shoulder radius R_{fc}, higher level of stenosis S_r, low fibrous cap thickness f_c, moderate lipid core thickness W_c, and consequently also low percentage (K_{ax},K_{circ}) of the lipid core and low lipid core radius R_c; the lipid cores with low R_c values infringe the shoulder region, see Fig. 4. Interestingly, the high σ_{cap} was observed in geometries with f_c up to 0.13 mm.

4. Discussion

In this preliminary parametric study, we have investigated which morphological features of the plaque are associated with high cap stress. Our model respects the shrank zero-pressure configuration and axial pre-stretch. Consequently, the values of geometric parameters refer to the loaded state and can be directly compared with real geometries recorded via CT-A or MRI.

Comparative analysis of the geometries generating high and low σ_{cap} values (see Table 3) revealed that low f_c increases the stress; this was expected in agreement with other studies [14,18,19]. More interestingly, a typical risky geometry is also associated with high stenosis ratio S_r, only a moderate lipid core volume (characterized

by W_c, K_{ax}, K_{circ}), and with interference of the lipid core with the shoulder region (characterized by $R_{fc} > R_c$ causing the interference of stress concentrations from both radiuses). Based on these results, we have specified typical cross sections of safe and risky plaques as shown in Fig. 4. The estimated shape of a risky plaque is in very good agreement with other studies – see for instance Fig. 4 in Kok et al. [16] or Fig. 2 in Cheng et al. study [17]. Therein, the highest stress [16] or rupture [17] occur at locations with a relatively thin lipid core if this core reaches the shoulder region with a low shoulder radius R_{fc}. Moreover, the stresses at this site are higher compared to the remainder of the shoulder region without the lipid core.

Further comparison shows that the observed cap thickness dispersion of 0.02 mm $< f_c <$ 0.13 mm in the plaques characterized by high σ_{cap} is in perfect agreement with histological observations [33]. Finally, it was shown that 70% of ruptured plaques contain lipid core characterized by $K_{circ} < 50\%$ [34] which is also in qualitative agreement with our results characterizing the vulnerable plaques by a smaller K_{circ}(median = 25%) and the less dangerous plaques by a very large K_{circ}(median = 62%) as shown in Table 3.

All the results of this preliminary study must be regarded with respect to their limitations. Besides the use of idealized geometry, it is noted that we used isotropic material model for the intima, because local orientation of the principal material directions in the atherosclerotic plaque is currently unknown. Further it is noted we prescribed the same material properties for the whole intima; thus we have omitted its specific properties under the atheroma; this was due to the low number of samples tested by Holzapfel et al. [26]. The model also neglects the spatial variability of mechanical properties of the diseased intima [35]; however, a strong correlation in PWS between models with homogeneous and heterogeneous intima was reported by Akyildiz et al. [10], thus we do not expect a significant impact of its heterogeneity on our conclusions. Also application of spatially constant pressure might be considered as a limitation since FSI analysis could provide a more realistic pressure map. However, these analyses are much more computationally demanding, and the pressure drop observed due to the presence of atherosclerotic plaque was shown to be negligible [7]. Finally, we did not include calcifications although they are known to have a significant effect on the wall stress in atherosclerotic plaques because they can hardly be modeled parametrically in 3D.

5. Conclusion

We have found that the risky plaque geometries can be – besides the fibrous cap thickness f_c– characterized by (i) a high level of stenosis S_r, (ii) only a moderately large lipid core (described by K_{ax} and K_{circ}), (iii) a combination of large shoulder radius R_{fc} and small lipid core radius R_c; under these conditions the lipid core reaches the shoulder region of the fibrous cap and increases here the stress concentration. These morphological features are usually several times larger than the fibrous cap thickness and thus they are easier to be estimated from CT-A or MRI. Further studies should confirm these observations on real plaques.

Competing interests

None declared.

Funding

This work is an output of Czech Science Foundation project No. 18-13663S.

Ethical approval

Not required.

References

[1] Sakakura K, Nakano M, Otsuka F, Ladich E, Kolodgie FD, Virmani R. Pathophysiology of atherosclerosis plaque progression. Hear Lung Circ 2013;22:399–411. doi:10.1016/j.hlc.2013.03.001.
[2] Fisher M, Paganini-Hill A, Martin A, Cosgrove M, Toole JF, Barnett HJM, et al. Carotid plaque pathology. Stroke 2005;36.
[3] Kochanek KD, Murphy SL, Xu J, Tejada-Vera B. Deaths: final data for 2014. Natl Vital Stat Rep 2016;65:1–122.
[4] Creager MA, Kaufman JA, Conte MS. Acute limb ischemia. N Engl J Med 2012;23366:2198–206.
[5] Holzapfel GA, Mulvihill JJ, Cunnane EM, Walsh MT. Computational approaches for analyzing the mechanics of atherosclerotic plaques: a review. J Biomech 2014;47:859–69. doi:10.1016/j.jbiomech.2014.01.011.
[6] Wang L, Tang D, Maehara A, Wu Z, Yang C, Muccigrosso D, et al. Fluid-structure interaction models based on patient-specific IVUS at baseline and follow-up for prediction of coronary plaque progression by morphological and biomechanical factors: a preliminary study. J Biomech 2018;68:43–50. doi:10.1016/J.JBIOMECH.2017.12.007.
[7] Chhai P, Lee JH, Rhee K. Effects of longitudinal asymmetric distribution of a lipid core on plaque wall stress. J Biomech Sci Eng 2017;12 16-00588-16-00588. doi:10.1299/jbse.16-00588.
[8] Cilla M, Borrás I, Peña E, Martínez MA, Malvè M. A parametric model for analysing atherosclerotic arteries: on the FSI coupling. Int Commun Heat Mass Transf 2015;67:29–38. doi:10.1016/j.icheatmasstransfer.2015.06.017.
[9] Fan R, Tang D, Yang C, Zheng J, Bach R, Wang L, et al. Human coronary plaque wall thickness correlated positively with flow shear stress and negatively with plaque wall stress: an IVUS-based fluid-structure interaction multi-patient study. Biomed Eng Online 2014:32. doi:10.1186/1475-925X-13-32.
[10] Akyildiz AC, Speelman L, van Velzen B, Stevens RRF, van der Steen AFW, Huberts W, et al. Intima heterogeneity in stress assessment of atherosclerotic plaques. Interface Focus 2018;8 20170008. doi:10.1098/rsfs.2017.0008.
[11] Nieuwstadt HA, Akyildiz AC, Speelman L, Virmani R, van der Lugt A, van der Steen AFW, et al. The influence of axial image resolution on atherosclerotic plaque stress computations. J Biomech 2013;46:689–95. doi:10.1016/j.jbiomech.2012.11.042.
[12] Nieuwstadt HA, Kassar ZAM, Van Der Lugt A, Breeuwer M, Van Der Steen AFW, Wentzel JJ, et al. A computer-simulation study on the effects of MRI voxel dimensions on carotid plaque lipid-core and fibrous cap segmentation and stress modeling. PLoS One 2015;10:1–15. doi:10.1371/journal.pone.0123031.
[13] Huang Y, Teng Z, Sadat U, Hilborne S, Young VE, Graves MJ, et al. Non-uniform shrinkage for obtaining computational start shape for in-vivo MRI-based plaque vulnerability assessment. J Biomech 2011;44(12):2316–19. doi:10.1016/j.jbiomech.2011.06.014.
[14] Cilla M, Peña E, Martínez MA. 3D computational parametric analysis of eccentric atheroma plaque: influence of axial and circumferential residual stresses. Biomech Model Mechanobiol 2012;11:1001–13. doi:10.1007/s10237-011-0369-0.
[15] Li ZY, Howarth S, Trivedi RA, U-King-Im JM, Graves MJ, Brown A, et al. Stress analysis of carotid plaque rupture based on in vivo high resolution MRI. J Biomech 2006;39:2611–22. doi:10.1016/j.jbiomech.2005.08.022.
[16] Kok AM, Speelman L, Virmani R, van der Steen AFW, Gijsen FJH, Wentzel JJ. Peak cap stress calculations in coronary atherosclerotic plaques with an incomplete necrotic core geometry. Biomed Eng Online 2016:1–13. doi:10.1186/s12938-016-0162-5.
[17] Cheng GC, Loree HM, Kamm RD, Fishbein MC, Lee RT. Distribution of circumferential stress in ruptured and stable atherosclerotic lesions. A structural analysis with histopathological correlation. Circulation 1993;87:1179–87. doi:10.1161/01.CIR.87.4.1179.
[18] Loree HM, Kamm RD, Stringfellow RG, Lee RT. Effects of fibrous cap thickness on peak circumferential stress in model atherosclerotic vessels. Circ Res 1992;71:850–8. doi:10.1161/01.RES.71.4.850.
[19] Ohayon J, Finet G, Gharib AM, Herzka DA, Tracqui P, Heroux J, et al. Necrotic core thickness and positive arterial remodeling index: emergent biomechanical factors for evaluating the risk of plaque rupture. Am J Physiol Hear Circ Physiol 2008;295:H717–27.
[20] Lee W, Choi GJ, Cho SW. Numerical study to indicate the vulnerability of plaques using an idealized 2D plaque model based on plaque classification in the human coronary artery. Med Biol Eng Comput 2016:1–9. doi:10.1007/s11517-016-1602-x.
[21] Gijsen FJH, Nieuwstadt HA, Wentzel JJ, Verhagen HJM, van der Lugt A, van der Steen AFW. Carotid plaque morphological classification compared with biomechanical cap stress: implications for a magnetic resonance imaging-based assessment. Stroke 2015;46:2124–8. doi:10.1161/STROKEAHA.115.009707.
[22] Holzapfel GA, Sommer G, Regitnig P, Zheng J, Bach R, Wang L, et al. Anisotropic mechanical properties of tissue components in human atherosclerotic plaques. J Biomech Eng 2004;126:657. doi:10.1115/1.1800557.
[23] Holzapfel GA, Stadler M, Gasser TC. Changes in the mechanical environment of stenotic arteries during interaction with stents: computational assessment of parametric stent designs. J Biomech Eng 2005;127:166. doi:10.1115/1.1835362.

[24] Schriefl AJ, Zeindlinger G, Pierce DM, Regitnig P, Holzapfel G a. Determination of the layer-specific distributed collagen fibre orientations in human thoracic and abdominal aortas and common iliac arteries. J R Soc Interface 2012;9:1275–86. doi:10.1098/rsif.2011.0727.
[25] Holzapfel GA, Gasser TC, Ogden RW. A new constitutive framework for arterial wall mechanics and a comparative study of material models. J Elast 2000;61:1–48. doi:10.1023/A:1010835316564.
[26] Holzapfel GA, Sommer G, Regitnig P. Anisotropic mechanical properties of tissue components in human atherosclerotic plaques. J Biomech Eng 2004;126:657–65. doi:10.1115/1.1800557.
[27] Tang D, Yang C, Mondal S, Liu F, Canton G, Hatsukami TS, et al. A negative correlation between human carotid atherosclerotic plaque progression and plaque wall stress: in vivo MRI-based 2D/3D FSI models. J Biomech 2008;41:727–36. doi:10.1016/j.jbiomech.2007.11.026.
[28] Ansys Inc. ANSYS 17.2. userś manual 2017.
[29] Riveros F, Chandra S, Finol EA, Gasser TC, Rodriguez JF. A pull-back algorithm to determine the unloaded vascular geometry in anisotropic hyperelastic AAA passive mechanics. Ann Biomed Eng 2013;41:694–708. doi:10.1007/s10439-012-0712-3.
[30] Belytschko T, Liu WK, Wing K, Moran B (Brian). Nonlinear finite elements for continua and structures. 2nd ed. Wiley Subscription Services, Inc., A Wiley Company; 2013.
[31] McKay MD, Beckman RJ, Conover WJ. Comparison of Three Methods for Selecting Values of Input Variables in the Analysis of Output from a Computer Code. Technometrics 1979;21:239–45. doi:10.1080/00401706.1979.10489755.
[32] Mann HB, Whitney DR. On a Test of whether one of two random variables is stochastically larger than the other. Ann Math Stat 1947;18:50–60. doi:10.2307/2236101.
[33] Tanaka A, Imanishi T, Kitabata H, Kubo T, Takarada S, Tanimoto T, et al. Morphology of exertion-triggered plaque rupture in patients with acute coronary syndrome an optical coherence tomography study. Circulation 2008;118(23):2368–73. doi:10.1161/CIRCULATIONAHA.108.782540.
[34] Burke AP, Virmani R, Galis Z, Haudenschild CC, Muller JE. Task force #2—what is the pathologic basis for new atherosclerosis imaging techniques? J Am Coll Cardiol 2003;41:1874–86. doi:10.1016/S0735-1097(03)00359-0.
[35] Wang Q, Canton G, Guo J, Guo X, Hatsukami TS, Billiar KL, et al. MRI-based patient-specific human carotid atherosclerotic vessel material property variations in patients, vessel location and long-term follow up. PLoS One 2017;12:e0180829. doi:10.1371/journal.pone.0180829.